Postprint version of paper published in Food Microbiology 2015, vol. 45(B), p. 179-188.
The content is identical to the published paper, but without the final typesetting by the publisher.

An individual-based modeling approach to simulate the effects of cellular nutrient competition on *Escherichia coli* K-12 MG1655 colony behavior and interactions in aerobic structured food systems

Ignace L.M.M. TACK[a], Filip LOGIST[a], Estefanía NORIEGA FERNÁNDEZ[a], Jan F.M. VAN IMPE[a]

[a] *CPMF² - Flemish Cluster Predictive Microbiology in Foods – www.cpmf2.be*

OPTEC - Center of Excellence Optimization in Engineering – www.kuleuven.be/optec

BioTeC - Chemical and Biochemical Process Technology and Control,

Department of Chemical Engineering, KU Leuven,

Willem de Croylaan 46 box 2423, B-3001 Leuven, Belgium.

[ignace.tack, filip.logist, estefania.noriegafernandez, jan.vanimpe]@cit.kuleuven.be

*** Corresponding author:**

Jan F.M. Van Impe

BioTeC - Chemical and Biochemical Process Technology and Control

Department of Chemical Engineering, KU Leuven

Willem de Croylaan 46 box 2423, B-3001 Leuven, Belgium.

Tel.: +32 16 32 14 66

Fax: +32 16 32 29 91

E-mail address: jan.vanimpe@cit.kuleuven.be

Journal homepage: http://www.sciencedirect.com/science/journal/07400020
Original file available at: http://www.sciencedirect.com/science/article/pii/S0740002014000963

Postprint version of paper published in Food Microbiology 2015, vol. 45(B), p. 179-188.
The content is identical to the published paper, but without the final typesetting by the publisher.

Abstract

Traditional kinetic models in predictive microbiology reliably predict macroscopic dynamics of planktonically-growing cell cultures in homogeneous liquid food systems. However, most food products have a semi-solid structure, where microorganisms grow locally in colonies. Individual colony cells exhibit strongly different and non-normally distributed behavior due to local nutrient competition. As a result, traditional models considering average population behavior in a homogeneous system do not describe colony dynamics in full detail.

To incorporate local resource competition and individual cell differences, an individual-based modeling approach has been applied to *Escherichia coli* K-12 MG1655 colonies, considering the microbial cell as modeling unit.

The first contribution of this individual-based model is to describe single colony growth under nutrient-deprived conditions. More specifically, the linear and stationary phase in the evolution of the colony radius, the evolution from a disk-like to branching morphology, and the emergence of a starvation zone in the colony center are simulated and compared to available experimental data. These phenomena occur earlier at more severe nutrient depletion conditions, i.e., at lower nutrient diffusivity and initial nutrient concentration in the medium. Furthermore, intercolony interactions have been simulated. Higher inoculum densities lead to stronger intercolony interactions, such as colony merging and smaller colony sizes, due to nutrient competition.

This individual-based model contributes to the elucidation of characteristic experimentally observed colony behavior from mechanistic information about cellular physiology and interactions.

Keywords

predictive microbiology; structured food model systems; microbial colony dynamics; microbial intracolony and intercolony interactions; individual-based modeling; Repast Simphony

Journal homepage: http://www.sciencedirect.com/science/journal/07400020
Original file available at: http://www.sciencedirect.com/science/article/pii/S0740002014000963

Postprint version of paper published in Food Microbiology 2015, vol. 45(B), p. 179-188.
The content is identical to the published paper, but without the final typesetting by the publisher.

1. Introduction

In the food industry, accurate control of microbiological quality and safety is indispensable. Predictive microbiology provides a theoretical framework for this purpose by developing mathematical models to describe and predict microbial dynamics under various environmental conditions (Buchanan, 1993). Traditional models applied in food industry are often constructed as deterministic low-complexity systems of coupled differential or algebraic equations (e.g., Baranyi and Roberts, 1994). These equation systems accurately predict macroscopic dynamics of microbial populations with similarly behaving microorganisms, such as the global cell density of pure exponential-phase cultures in homogeneous liquids.

However, most food products consist of a semi-solid structure restricting microbial mobility. This restriction forces microorganisms to grow locally in colonies. Over time, the relatively high cell density in these colonies results in local competition for space and nutrients between neighboring microorganisms. In addition, under oxygen-limited environmental conditions microorganisms excrete acid metabolite products into the surrounding medium (Clark, 1989). Consequently, due to diffusion limitations of nutrients and metabolites, the colony center is characterized by nutrient depletion and acidification, and concomitant cell starvation (Wimpenny et al., 1995; Malakar et al., 2000). Hence, cells exhibit strongly different individual behavior according to their position along the colony radius. As a matter of fact, the traditional macroscopic models are not appropriate to describe microbial dynamics in structured systems as these do not incorporate local differences and interactions between the individual cells.

To take these mutual interactions and individual differences into account, colony dynamics are described by means of an *individual-based model* (*IbM*). Individual-based models describe global dynamics of a system in terms of its composing individuals or agents. In this specific case, the microbial cell is considered as the basic modeling unit. In other words, global colony dynamics are not implemented explicitly, but emerge from processes at the microscopic cellular level.

Journal homepage: http://www.sciencedirect.com/science/journal/07400020
Original file available at: http://www.sciencedirect.com/science/article/pii/S0740002014000963

Several microbiological IbMs are already available to simulate specific microbial colony behaviors (Kreft et al., 1998; Ginovart et al., 2002; Mabrouk et al., 2010). However, these models are either difficult to install and use, apply parameter values from different *Escherichia coli* strains, contain parameters without quantitative biological or physical meaning, or do not incorporate the effect of nutrient depletion and cell starvation on intracellular processes, such as DNA replication and cell division. Therefore, based on the BacSim model of Kreft et al. (1998), the MICRODIMS IbM has been developed at the KU Leuven/BioTeC research group (Verhulst et al., 2011). The basic version of MICRODIMS simulates the lag phase and exponential growth of aerobic colonies in a nutrient-rich and homogeneous medium without acid metabolite excretion and nutrient diffusion limitations. In this paper, this basic module is extended to reproduce behavior and interactions of monolayer colonies subject to diffusion limitations in a two-dimensional aerobic environment. Growth of *E. coli* K-12 MG1655 cells in gel media is considered as a specific case study, as cellular parameter values and experimental observations are largely available for this particular *E. coli* strain.

2. Material and methods

In this section, the extended version of MICRODIMS is described according to the widely-used *ODD* protocol (Grimm et al., 2010). This protocol divides the IbM description in three parts: *Overview*, *Design Concepts* and *Details*.

2.1 Overview

2.1.1 Purpose

The purpose of this model is to simulate mesoscopic dynamics of a monolayer colony of *Escherichia coli* K-12 MG1655 in a homogeneous gel medium under aerobic conditions. Firstly, single colony dynamics are simulated, together with the influence of nutrient diffusivity and initial nutrient concentration. Secondly, intercolony interactions are investigated.

2.1.2 Entities, state variables, and scales

The model has two categories of entities: microbial cells and environment.

Microbial cells are represented as a circle. Each cell is characterized by a radius, mass, spatial position in the environment, and maximum specific cellular growth rate. In addition, it is situated in a specific stage of the cell reproduction cycle and has a specific number of ongoing DNA replication cycles. The progress of these replication cycles is stored in an internal list variable. Finally, the color of the cell indicates its activity level; growing microorganisms are green, starving cells turn red.

The two-dimensional environment represents a 1 mm x 1 mm part of the gel system. It is discretized in equally-sized square units. Each square patch is characterized by a glucose nutrient concentration. As the simulation of local nutrient competition between individual cells is a primary goal, the patch dimension is selected to be in the same order of magnitude as the microorganism size, more specifically 2 µm (Kreft et al., 1998).

2.1.3 Process overview and scheduling

The IbM contains four types of processes: intracellular processes, interactions between the cell and its surrounding medium, direct intercellular interactions, and diffusion processes in the medium.

The intracellular processes are cell growth, cell maintenance, DNA replication and cell division, and cell starvation. In order to sustain cell growth and other active intracellular processes, cellular glucose uptake from the surrounding medium is required. Excretion of acid metabolites is not incorporated in the model as there is no oxygen limitation and, accordingly, no release of acid metabolites into the medium. Microbial cells interact directly by repulsing neighboring cells in case of spatial overlap. Finally, local glucose uptake causes glucose concentration gradients in the environment with concomitant glucose diffusion throughout the medium.

In the model implementation, two time resolutions are applied: a smaller time step t_1 of 0.0005 min for processes with fast dynamics (i.e., the diffusion and uptake process) and a larger time step t_2 of

0.1 min for cellular functions with slower dynamics (all the other processes). The slow processes are executed first in the following order: biomass growth and cell maintenance, cell starvation, DNA reproduction and cell division, and finally cell repulsion. Afterwards, the diffusion process levels glucose concentration gradients caused by nutrient uptake. Each time step, the list of microorganisms is shuffled to avoid favoritism with respect to nutrient uptake.

2.2 Design concepts

2.2.1 Emergence

Glucose depletion emerges from local intercellular competition for this nutrient. This nutrient overconsumption influences growth, starvation and reproduction of microbial cells in the colony center. Mesoscopic colony dynamics arise from this interplay between local glucose scarcity and individual cell behavior.

2.2.2 Sensing

The simulated cells are able to sense the glucose concentration of the environmental patch in which they are located. Cellular glucose uptake from the environment is adjusted with respect to this local nutrient availability. In addition, microorganisms detect overlap with neighboring cells. Finally, a cell is assumed to “know” its mass to control its substrate uptake, growth and maintenance, starvation, and DNA replication.

2.2.3 Interaction

Repulsion of neighboring cells upon spatial overlap is an example of a direct intercellular interaction. Competition for nutrient is an indirect interaction between microbial cells mediated by the environment.

2.2.4 Stochasticity

The model contains two sources of stochasticity: the direction in which daughter cells are positioned after cell division, and a stochastic element on the specific cellular growth rate to take into account growth asynchrony between cells.

2.2.5 Outputs

To verify the qualitative model validity with respect to experimental data, the evolution of the colony radius and morphology is simulated. Furthermore, the number of growing and starving cells is observed in order to infer the dynamics of the starvation zone in the colony center. Finally, the dynamic distribution of the specific cellular growth rate is plotted as a histogram.

2.3 Details

2.3.1 Initialization

At the start of the simulation, one microbial cell is positioned in the middle of the square environment that has a homogeneous initial glucose concentration $C_{S,init}$ of 0.1 or 1.0 g/L (Kreft et al., 1998). The initial volume of this inoculum cell is equal to the cell volume required to initiate the first DNA replication process (see Section 2.3.3.4).

2.3.2 Boundary conditions

Two types of environmental boundary conditions are implemented. In the first instance, simulations are executed with constant boundary conditions, i.e., the glucose concentration is held constant at its initial value at the environment borders: $C_{S,b} = C_{S,init}$ with $C_{S,b}$ the glucose concentration at the boundaries of the environment. This implies that the environment is surrounded by an infinitely large nutrient reservoir without glucose diffusion limitations, which is a good approximation for case studies in which the distance between inoculum cells is large with respect to the dimension of the considered environment.

However, when inoculum cell density increases and, consequently, intercellular distance decreases, this approximation is no longer valid. For higher inoculum cell densities, it is more appropriate to apply periodic boundary conditions, i.e., the flux through a boundary is equal to the flux through the opposite boundary: $J_b = J_{b'}$, with J_b the flux through an environment boundary, and $J_{b'}$ the flux through the opposite boundary. Implications of these two different boundary conditions on the simulation outcomes are detailed in Section 3.1.3.

2.3.3 Submodels

2.3.3.1 Nutrient diffusion

Glucose diffusion is modeled by means of the second law of Fick in two dimensions. For 2D isotropic media, this law is mathematically expressed as

$$\frac{\partial C_S}{\partial t} = D_S \cdot \left(\frac{\partial^2 C_S}{\partial x^2} + \frac{\partial^2 C_S}{\partial y^2}\right), \tag{1}$$

with C_S [fg/fL] the glucose concentration, D_S [µm²/min] the diffusion coefficient of glucose in the structured medium, x [µm] and y [µm] the two spatial dimensions, and t [min] the time. Unfortunately, for the applied initial and boundary conditions, this partial differential equation has no analytical solution. Therefore, the environment is divided into discrete units, as mentioned in Section 2.1.2, in order to solve the PDE numerically as a difference equation.

Various numerical discretization algorithms have been developed for this PDE. The most appropriate numerical scheme is selected as a trade-off between required simulation run time, numerical stability, and accuracy. In this case, the Alternating Direction Implicit (ADI) scheme of Peaceman and Rachford (1955) is applied, as it is an unconditionally stable diffusion scheme with a second-order accuracy in both time and space dimensions. The ADI implementation consists of two stages:

$$\left(1 - \frac{D_S}{2} \cdot \frac{\Delta t}{(\Delta x)^2} \cdot \delta_x^2\right) C_{S,(i,j)}\left(t + \frac{\Delta t}{2}\right) = \left(1 + \frac{D_S}{2} \cdot \frac{\Delta t}{(\Delta y)^2} \cdot \delta_y^2\right) C_{S,(i,j)}(t), \tag{2}$$

$$\left(1 - \frac{D_S}{2} \cdot \frac{\Delta t}{(\Delta y)^2} \cdot \delta_y^2\right) C_{S,(i,j)}(t + \Delta t) = \left(1 + \frac{D_S}{2} \cdot \frac{\Delta t}{(\Delta x)^2} \cdot \delta_x^2\right) C_{S,(i,j)}\left(t + \frac{\Delta t}{2}\right), \tag{3}$$

with $C_{S,(i,j)}(t)$ [fg/fL] the glucose concentration at time t in the discrete environmental unit with coordinates (i,j), and the second order central differences

$$\delta_x^2 C_{S,(i,j)}(t) = C_{S,(i+1,j)}(t) - 2C_{S,(i,j)}(t) + C_{S,(i-1,j)}(t), \quad (4)$$

$$\delta_y^2 C_{S,(i,j)}(t) = C_{S,(i,j+1)}(t) - 2C_{S,(i,j)}(t) + C_{S,(i,j-1)}(t). \quad (5)$$

Both steps lead to a tridiagonal system of linear equations, solved by the computationally efficient Thomas algorithm (Thomas, 1949). Note that the spatial discretization step in the horizontal and vertical direction are the same (Δx = Δy).

The nutrient diffusion coefficient D_S is influenced by the gel matrix structure. At a temperature of 37°C, the diffusion coefficient of glucose in a 5% (w/w) agarose gel is equal to $6.7925 \cdot 10^{-10}$ m²/s or 40755 µm²/min (Andersson and Öste, 1994), approximately 75% of the glucose diffusivity in water at the same temperature. To investigate the influence of lower diffusivities, some simulations are executed with a tenfold lower diffusion coefficient.

2.3.3.2 Cellular metabolism

Nutrient uptake

Cellular glucose uptake from the environment, required for cell growth and maintenance, is modeled by means of the Monod kinetic model (Monod, 1942):

$$-\frac{\Delta S_{k,(i,j)}}{\Delta t} = v_{k,(i,j)} = v_{k,max} \cdot \frac{C_{S,(i,j)}}{K_S + C_{S,(i,j)}} = \frac{\mu_{k,max}}{Y_{X/S}} \cdot \frac{C_{S,(i,j)}}{K_S + C_{S,(i,j)}} \cdot X_k. \quad (6)$$

In this formula, $C_{S,(i,j)}$ [fg/fL] is the nutrient concentration of the environmental unit in which the microbial cell is situated, $\Delta S_{k,(i,j)}$ [fg] the glucose uptake by cell k from its environment, v_k [fg/min] the glucose uptake rate of cell k, $v_{k,max}$ [fg/min] the maximum nutrient uptake rate, K_S [fg/fL] the Monod half-saturation constant, $\mu_{k,max}$ [min^{-1}] the maximum specific cellular growth rate, $Y_{X/S}$ [fgDW/fg] the cellular yield coefficient of biomass on glucose, and X_k [fgDW] the mass of cell k. If the glucose amount in environmental unit (i,j) is smaller than $\Delta S_{k,(i,j)}$, the nutrient uptake reduces to the available

amount of glucose and the concentration of the environmental patch is set to zero. It should be noted that the specific cellular growth rate μ_k is not equal to the specific growth rate μ commonly known as a parameter at the microbial population level. Both parameters can be linked as follows:

$$\frac{\mathrm{d}X}{\mathrm{d}t} = \mu \cdot X = \left(\mu_1 \cdot \frac{X_1}{X} + \mu_2 \cdot \frac{X_2}{X} + \cdots + \mu_n \cdot \frac{X_n}{X}\right) \cdot X,$$

with *X* the biomass of the whole microbial population, and n the number of cells in this population.

To take asynchrony in cell growth and division into account, the maximum specific cellular growth rate is composed of a deterministic and stochastic part *e*:

$$\mu_{k,max} = \mu_{max,m} \cdot (1 + e), \tag{7}$$

with $\mu_{max,m}$ [min^{-1}] the mean maximum specific cellular growth rate over all the cells, and *e* [-] a normally-distributed number with zero mean value and constant variance. It is assumed that the mean maximum specific cellular growth rate is equal to the maximum specific growth rate of a whole microbial population, μ_{max}. Numerical values for the parameters in the nutrient uptake process and the coefficient of variation *CV* for $\mu_{k,max}$ are included in Table 1.

Cell growth and maintenance

In the first instance, consumed glucose is utilized for cell maintenance. When cell maintenance requirements are met, the excess of assimilated glucose is directed to biomass production. If the maintenance processes are not saturated by the available nutrient, the deficit in glucose uptake is compensated by degrading an equivalent amount of cell mass.

This cellular growth and maintenance behavior is implemented as an exponential growth law, containing contributions of Monod-type nutrient uptake, and biomass degradation according to the Herbert model (Herbert, 1958):

$$\frac{\Delta X_k}{\Delta t} = \mu_k \cdot X_k = v_{k,(i,j)} \cdot Y_{X/S} - m \cdot X_k \cdot Y_{X/S} = \left(\mu_{k,max} \cdot \frac{C_{S,(i,j)}}{K_S + C_{S,(i,j)}} - m \cdot Y_{X/S}\right) \cdot X_k, \tag{8}$$

with μ_k [min^{-1}] the specific cellular growth rate of microbial cell *k*, and *m* [fg/(fgDW·min)] the specific maintenance coefficient.

2.3.3.3 Cell starvation

Microbial cells starve when their maintenance requirements are not met and, consequently, their specific cellular growth rate is negative. Starving cells change color from green to red in the simulation. DNA replication and cell division processes, addressed in the next subparagraph, stop progressing in starving cells.

2.3.3.4 DNA replication and cell reproduction

Cell reproduction cycles

Before cells divide in two daughter organisms, they replicate their genetic information. The cell cycle phase in which DNA is replicated, is called the *C*-phase (Maaløe and Kjeldgaard, 1966). This *C*-phase is followed by a *D*-phase in which the produced sister chromosomes segregate towards the cell poles. At the end of the *D*-phase, a microorganism divides at mid-cell in two equally large daughter cells.

Cooper and Helmstetter (1968) observed that the *C*- and *D*-period of *E. coli* B/r have a constant duration of 40 min and 20 min respectively, regardless from specific cellular growth rate in a range from 0.8 h^{-1} to 1.9 h^{-1}. However, more recent research studies (Helmstetter, 1996; Michelsen et al., 2003) have shown that the constancy of the *C*+*D*-period duration does not hold outside this range. At specific cellular growth rates below 0.011 min^{-1} (0.66 h^{-1}), the duration of the *C*+*D*-period [min] increases according to the following mathematical expression:

$$C + D = 3.50 \cdot \mu_k^{-0.658} \qquad \text{for } 0 \le \mu_k \le 0.011 \text{ min}^{-1}, \tag{9}$$

$$C + D = 67.92 \qquad \text{for } \mu_k > 0.011 \text{ min}^{-1}, \tag{10}$$

fitted to the experimental data of Helmstetter (1996) and Michelsen et al. (2003). This equation is graphically represented in Figure 1.

Initiation of the cell reproduction cycle

Donachie (1968) derived that the *C*-phase is initiated at a critical ratio *X** [fgDW] of cell mass to the number of ongoing DNA replications. Accordingly, cell masses X_{init} at which the DNA replication is initiated are

$$\frac{X_{init}}{n_i} = X^* \Rightarrow X_{init} = X^* \cdot n_i = X^* \cdot 2^j \text{ with } j = 0, 1, 2, \ldots \quad (11)$$

For exponentially growing cultures, the critical initiation ratio can be derived from the cell mass at division X_D [fgDW] (Dens et al., 2005):

$$X_D(\mu_k) = X^* \cdot \exp\left(\mu_k \cdot (C + D)\right) \quad (12)$$

$$\Rightarrow X^* = \frac{2X_B}{\exp\left(\mu_k \cdot (C+D)\right)} = \frac{2\rho_{DW} \cdot V_m}{\alpha \cdot \exp\left(\mu_k \cdot (C+D)\right)}. \quad (13)$$

In this equation, V_m [fL] is the mean cell volume, X_B [fgDW] the cell mass at birth, ρ_{DW} [fgDW/fL] the density of dry cell mass, and α [-] the ratio of the mean cell mass to the cell mass at birth. This α ratio has a value of 1.377 for cells with a specific growth rate *CV* of 0.10 (Koch, 1993).

Although Donachie (1968) postulated that the critical ratio was a constant, Wold et al. (1994) observed a linear decrease of *X** as a function of the specific growth rate:

$$X^*(\mu_k) = A - B \cdot \mu_k, \text{ or} \quad (14)$$

$$V_m(\mu_k) = \frac{\alpha \cdot \exp\left(\mu_k \cdot (C+D)\right)}{2\rho_{DW}} \cdot (A - B \cdot \mu_k). \quad (15)$$

Values of the *A* and *B* constant, respectively 610.7 fgDW and 8315.1 fgDW·min, have been determined by fitting the last equation to the mean cell volume data of Volkmer and Heinemann (2011), as shown in Figure 2(a). Figure 2(b) shows that, the critical initiation ratio *X** decreases approximately twofold in a specific growth rate span of 0.03 min^{-1}, which corresponds to observations by Wold et al. (1994).

Implementation of the cell reproduction cycles

Information about ongoing replication cycles is stored in an internal list variable. Each list entry has a value from 1.0 to 0 and represents the already fulfilled fraction of the corresponding replication cycle. Every time step, the elements of the internal list are updated as follows:

$$e_{new} = e_{old} - \frac{\Delta t}{C+D}, \tag{16}$$

with e_{new} and e_{old} the new and old value of the element, respectively.

When a cell attains the critical initiation ratio, a new reproduction cycle is initiated by appending an entry of 1.0 to the list variable. If the first list variables reaches a zero value, this entry is removed from the list and the cell divides. Daughter cells inherit remaining unaccomplished replication cycles.

2.3.3.5 Cell motility and organization

Cellular motility and, consequently, spreading of the microorganisms over the medium is hindered due to the structure of the medium. Microbial colonies expand by relaxing the internal pressure increase due to biomass growth. In MICRODIMS, this relaxation is effected by avoiding spatial overlap between neighboring organisms, implemented according to the cell shoving mechanism of Kreft et al. (1998).

In this cell shoving mechanism, for each individual cell, the vector sum of all positive overlap radii with neighboring microorganisms is calculated. The overlap radius r_o [µm] with a neighboring organism is defined as

$$r_o = s \cdot r_k + r_n - d, \tag{17}$$

with r_k [µm] and r_n [µm] the radius of the considered cell and its neighbor, d [µm] the distance between the centers of these two cells, and s [-] a factor to take into account a realistic minimum distance between neighboring cells.

2.4 Software implementation

The MICRODIMS model is implemented in the Repast Simphony software toolkit (North et al., 2013) using the object-oriented Java programming language within the Eclipse IDE. Repast Simphony provides a standard programming framework for the implementation of IbMs. Repast Simphony is selected over other software toolkits as its simulation speed is relatively fast, and because Java provides efficient array structures and for-loops to iterate over array elements. These features are required for an efficient implementation of the ADI diffusion scheme with the Thomas algorithm.

3. Results and discussion

In this section, experimentally observed microbial colony dynamics are simulated with the developed IbM. According to the work of Malakar et al. (2000), a distinction is made between the behavior of an isolated single colony with cellular interactions in the colony itself (*intracolony interactions*) and interactions between multiple colonies (*intercolony interactions*). Distinctive experimental features of single colony growth are the emergence of cell starvation in the center (Wimpenny et al., 1995), linear increase and stationary phase behavior of the radius (Kamath and Bungay, 1988; Wimpenny et al., 1995; Mitchell and Wimpenny, 1997), and a variety of morphologies (Matsushita et al., 1998). Observed intercolony interactions, such as colony repulsion (Matsushita and Fujikawa, 1990) or merging and colony size differences (Malakar et al., 2000), are influenced by the inoculum distances and density.

3.1 From intracolony cellular interactions to single colony dynamics

3.1.1 Local cellular nutrient competition and nutrient depletion in the colony center

Nutrient availability in the colony center decreases to a depleted level, due to the relatively high local cell density and nutrient diffusion limitations in the medium. The glucose depletion pattern is influenced by the nutrient diffusivity D_S and initial nutrient concentration $C_{S,init}$. At lower diffusion

coefficient or initial glucose concentration values, nutrient depletion emerges earlier in the simulation and, consequently, the microbial colonies are smaller (see Figure 3).

3.1.2 Mesoscopic colony behavior: colony morphology, radius and cell activity

Colony dynamics are not summarizable into a single scalar variable. Instead, three colony characteristics are observed: cell activity, radius, and morphology.

From the moment that glucose depletion is important enough to induce cell starvation (see Figure 4(a)), the ratio of starving to growing cells increases continuously over time, as illustrated in Figure 4(b). Ultimately, only the microorganisms in a small band at the colony boundary are able to take up nutrient and grow. Figure 3 and 4 illustrate that this band is broader at less severe nutrient depletion conditions. Growing and starving cells give rise to a bimodal distribution of the specific cellular growth rate, as presented in Figure 4(c). Mean specific colony growth rates can be derived from this dynamical distribution of specific cellular growth rates.

The colony radius is defined as the distance between the initial position of the inoculum cell and the microorganism furthest away from this position. Figure 5 illustrates that the evolution of the colony radius comprises a superlinear growth phase at the start of the simulation and a linear increase after the nutrient depletion effect becomes important. This evolution has been experimentally observed by Kamath and Bungay (1988), Wimpenny et al. (1995) and Mitchell and Wimpenny (1997). The transition from superlinear to linear radius increase coincides with the emergence of cell starvation (compare Figure 4 to Figure 5).

A gradual evolution from a circular to lobed morphology is perceived as nutrient depletion becomes more stringent and even affects the colony boundary region (Figure 6). Due to stochasticity in the cell motility mechanism, the individual cells are organized irregularly at the colony boundary. At low glucose diffusivities (D_S = 4075.5 µm²/min), the most externally-oriented cells screen other organisms at the colony boundary from nutrient uptake. This screening effect amplifies colony boundary irregularities, ultimately leading to a branched colony shape. At higher D_S and $C_{S,init}$ values, the lobed

Eden morphology has also been experimentally observed, albeit at a larger spatial scale, by Matsushita et al. (1998) and in our research group (Figure 6(d)).

3.1.3 Influence of spatial boundary conditions on stationary growth phase behavior

Constant boundary conditions represent the assumption that the environment is surrounded by an infinite homogeneous bulk medium at the initial glucose concentration. Consequently, fresh nutrient is constantly provided from this bulk reservoir, preventing the emergence of a stationary growth phase in the previous simulation. The assumption of an infinite nutrient reservoir is only valid if the inoculum cell density is low enough to ensure the absence of nutrient competition between colonies arising from different inoculum cells.

However, when the distance between inoculum cells is in the same order of magnitude as the dimensions of the square environment, it is more appropriate to apply periodic boundary conditions, as implemented by Mabrouk et al. (2010). In this case, the finite reservoir of available nutrient is as large as the considered square environment. A stationary growth phase emerges after the environment is completely depleted from nutrient, as shown in Figure 7. Taking into account that only 2 nL of the food system is modeled, the entire system contains approximately $0.5 \cdot 10^9$ cells per mL in the stationary phase. For *E. coli* K-12 MG1655 in BHI medium at 37°C and pH 7.0, experimental cell densities in the order of 10^9 CFU/mL are reached in the stationary phase (Noriega et al., 2013).

3.2 Intercolony interactions: influence of inoculum distances and density

Microbial colonies arising from closely neighboring inoculum cells compete locally for nutrient resources. If the space between the involved colonies gets depleted from nutrient before the colonies reach each other, a no-growth zone emerges between these colonies, as illustrated in Figures 8(a) and 8(c).

However, beneath a specific critical distance between the inoculum cells, the nutrient depletion pattern does not emerge fast enough to effect the no-growth zone, leading to a merge of the

interacting colonies (Figure 8(b)). The merging of microbial colonies has also been observed experimentally, as presented in Figure 8(d).

The influence of inoculum density has been investigated by varying the number of inoculum cells placed randomly in the environment. At high inoculum densities, glucose is depleted at a faster rate, leading to smaller colonies approaching planktonic growth. This result corresponds to the experimental results of Malakar et al. (2000). The maximum sustainable number of cells is approximately constant regardless of the inoculum density (see Figure 9), as experimentally observed by Jeanson et al. (2011).

3.3 Model limitations, utility and further extensions

As mentioned in the *Overview* part of the ODD protocol, this IbM describes the dynamics of an aerobic microbial monolayer in a 2D environment. As a result, this model is neither fully representative for submerged colony behavior inside food media, nor for growth of multilayered colonies on food surfaces.

However, this IbM is the first to qualitatively simulate some particular colony phenomena: (*i*) emergence of a starvation zone in the center, (*ii*) linear increase of the radius, (*iii*) stationary growth phase behavior, (*iv*) colony merging, and (*v*) the influence of inoculum density on colony size. In contrast to already existing IbMs for microbial colony dynamics, this model has the following advantages. Firstly, it is implemented in the state-of-the art and user-friendly Repast Simphony software toolkit containing basic functionalities for the implementation of IbMs. Secondly, nutrient diffusion is implemented by means of the ADI scheme with the computationally efficient Thomas algorithm. A third novelty is the incorporation of the cell starvation effect on DNA replication and cell division processes. In addition, each parameter has a quantitative biological or physical meaning and is hence experimentally measurable. Finally, it should be noted that most cellular parameter values are derived from experiments on *E. coli* K-12 MG1655 or other *E. coli* K-12 strains that are representative for this particular strain (Table 1).

Next modifications to MICRODIMS include the integration of acid metabolite excretion under oxygen-limited conditions, and the extension from a two-dimensional medium to an environment with three dimensions. These additions will render the IbM more representative for submerged colony dynamics, as described in Wimpenny et al. (1995), Mitchell and Wimpenny (1997), and Malakar et al. (2000). Metabolite excretion will be incorporated according to the concept of phenotype phase plane analysis (Edwards et al., 2001). The transition from a 2D to 3D environment requires a three-dimensional diffusion scheme, such as the LOD Crank-Nicolson method (Yanenko, 1971), and an adapted 3D cell shoving mechanism.

4. Conclusions

An individual-based model (IbM) has been implemented in the Repast Simphony software toolkit to describe the dynamics of microbial monolayer colonies. Single colony dynamics are qualitatively reproduced, such as the morphology evolution, linear radius increase, and emergence of a starvation zone in the center. The IbM demonstrates that these phenomena are caused by the interplay between local cellular glucose competition and nutrient diffusion limitations, ultimately leading to nutrient depletion.

In addition, interactions between different colonies are simulated. A no-growth zone emerges between two growing colonies due to nutrient depletion. However, if the inoculum cells of two colonies are located closely enough, these colonies will merge before the nutrient depletion pattern is fully developed. Intercolony distance is determined by the inoculum density, i.e., number of inoculum cells per surface unit. The simulation shows that, apart from determining colony merging behavior, inoculum density has an influence on the size of full-grown colonies. Higher inoculum densities lead to smaller colonies, as nutrient competition is more severe. However, inoculum density hardly affects the maximum sustainable number of cells in the medium.

Journal homepage: http://www.sciencedirect.com/science/journal/07400020
Original file available at: http://www.sciencedirect.com/science/article/pii/S0740002014000963

The merit of individual-based modeling in predictive microbiology is the elucidation of experimentally observed colony behavior in terms of cell physiological mechanisms and interactions. The incorporation of this knowledge in classical differential equation models will allow more accurate assessments of microbiological quality and safety in structured food products.

Acknowledgments

The research of I.L.M.M. Tack is funded by Ph.D. grant IWT SB-111565 of the Agency for Innovation by Science and Technology (IWT).

In addition, this work is supported by projects FWO-G.0930.13 and FWO KAN2013, 1.5.189.13 of the Research Foundation - Flanders (FWO), project PFV/10/002 (Center of Excellence OPTEC-Optimization in Engineering) of the KU Leuven Research Fund, Knowledge Platform KP/09/005 (SCORES4CHEM) of the KU Leuven Industrial Research Fund, and the Belgian Program on Interuniversity Poles of Attraction, initiated by the Belgian Federal Science Policy Office (IAP Phase VII - 19 DYSCO). J.F.M. Van Impe holds the chair Safety Engineering sponsored by the Belgian chemistry and life sciences federation essenscia.

References

Andersson, A.P., Öste, R.E., 1994. Diffusivity data of an artificial food system. Journal of Food Engineering, 23, 631-639.

Baranyi, J., Roberts, T.A., 1994. A dynamic approach to predicting bacterial growth in food. International Journal of Food Microbiology, 23, 277-294.

Baumler, D.J., Peplinski, R.G., Reed, J.L., Glasner, J.D., Perna, N.P., 2011. The evolution of metabolic networks of *E. coli*. BMC Systems Biology, 5: 182.

Buchanan, R.L., 1993. Predictive food microbiology. Trends in Food Science & Technology, 4, 6-11.

Clark, D.P., 1989. The fermentation pathways of *Escherichia coli*. FEMS Microbiology Reviews, 63, 223-234.

Cooper, S., Helmstetter, C.E., 1968. Chromosome replication and the division cycle of *Escherichia coli* B/r. Journal of Molecular Biology, 31, 519-540.

Dens, E.J., Bernaerts, K., Standaert, A.R., Van Impe, J.F., 2005. Cell division theory and individual-based modeling of microbial lag: Part I. The theory of cell division. International Journal of Food Microbiology, 101, 303-318.

Donachie, W.D., 1968. Relationship between cell size and time of initiation of DNA replication. Nature, 219, 1077-1079.

Edwards, J.S., Ramakrishna, R., Palsson, B.O., 2002. Characterizing the metabolic phenotype: A phenotype phase plane analysis. Biotechnology and Bioengineering, 77, 27-36.

Esquerré, T., Laguerre, S., Turlan, C., Carpousis, A.J., Girbal, L., Cocaign-Bousquet, M., 2013. Dual role of transcription and transcript stability in the regulation of gene expression in *Escherichia coli* cells cultured on glucose at different growth rates. Nucleic Acids Research, 41, 1-13.

Ginovart, M., López, D., Valls, J., 2002. INDISIM, an individual-based discrete simulation model to study bacterial cultures. Journal of theoretical microbiology, 214, 305-319.

Godin, M., Bryan, A.K., Burg, T.P., 2007. Measuring the mass, density, and size of particles and cells using a suspended microchannel resonator. Applied Physics Letters, 91, 123121.

Grimm, V., Berger, U., DeAngelis, D.L., Polhill, J.G., Giske, J., Railsback, S.F., 2010. The ODD protocol: A review and first update. Ecological modeling, 221, 2760-2768.

Helmstetter, C.E., 1996. Timing of synthetic activities in the cell cycle. In: Neidhardt, F.C., Curtiss III, F., Ingraham, R., Lin, J., Low, E., Magasanik, K., Reznikoff, W., Riley, M., Schaechter, M., Umbarger, H. (eds.). *Escherichia coli* and *Salmonella*: Cellular and molecular biology. 2nd ed. Washington, D.C.: ASM Press. Volume 2, Ch. 102, 1627-1637.

Herbert, D., 1958. Some principles of continuous culture. In: Tunevall, G. (ed.). Recent progress in microbiology, Symposia held at the VII International Congress on Microbiology, Stockholm. Uppsala: Almqvist & Wiksell, 381–396.

Ihssen, J., Grasselli, E., Bassin, C., François, P., Piffaretti, J.-C., Köster, W., Schrenzel, J., Egli, T., 2007. Comparative genomic hybridization and physiological characterization of environmental isolates indicate that significant (eco-)physiological properties are highly conserved in the species *Escherichia coli*. Microbiology, 153, 2052-2066.

Jeanson, S., Chadœuf, J., Madec, M.N., Aly, S., Floury, J., Brocklehurst, T.F., Lortal, S., 2011. Spatial distribution of bacterial colonies in a model cheese. Applied and Environmental Microbiology, 77, 1493-1500.

Kamath, R.S., Bungay, H.R., 1988. Growth of yeast colonies on solid media. Journal of General Microbiology, 134, 3061-3069.

Kamihira, M., Taniguchi M., Kobayashi, T., 1987. Sterilization of microorganisms with supercritical carbon dioxide. Agricultural and Biological Chemistry, 51(2), 407-412.

Koch, A.L., 1993. Biomass growth rate during the prokaryote cell cycle. Critical reviews in microbiology, 19, 17-42.

Kreft, J.-U., Booth, G., Wimpenny, J.W.T., 1998. Bacsim, a simulator for individual-based modeling of bacterial colony growth. Microbiology, 144, 3275-3287.

Maaløe, O., Kjeldgaard, N.O., 1966. Control of Macromolecular Synthesis. New York: W.A. Benjamin.

Mabrouk, N., Deffuant, G., Tolker-Nielsen, T., Lobry, C., 2010. Bacteria can form interconnected microcolonies when a self-excreted product reduces their surface motility: evidence from individual-based model simulations. Theory in Biosciences, 129, 1-13.

Malakar, P.K., Brocklehurst, T.F., Mackie, A.R., Wilson, P.D.G., Zwietering, M.H., van 't Riet, K., 2000. Microgradients in bacterial colonies: use of fluorescence ratio imaging, a non-invasive technique. International Journal of Food Microbiology, 56, 71-80.

Matsushita, M., Fujikawa, H., 1990. Diffusion-limited growth in bacterial colony formation. Physics A, 168, 498-506.

Matsushita, M., Wakita, J., Itoh, H., Ràfols, I., Matsuyama, T., Sakaguchi, H., Mimura, M., 1998. Interface growth and pattern formation in bacterial colonies. Physics A, 249, 517-524.

Michelsen, O., Teixeira de Mattos, M.J., Jensen, P.R., Hansen, F.G., 2003. Precise determinations of C and D periods by flow cytometry in *Escherichia coli* K-12 and B/r. Microbiology, 149, 1001-1010.

Mitchell, A.J., Wimpenny, J.W.T., 1997. The effects of agar concentration on the growth and morphology of submerged colonies of motile and non-motile bacteria. Journal of Applied Microbiology, 83, 76-84.

Monod, J. 1942. Recherches sur la croissance des cultures bactériennes. Hermann: Paris.

Nanchen, A., Schicker, A., Sauer, U., 2006. Nonlinear dependency of intracellular fluxes on growth rate in miniaturized continuous cultures of *Escherichia coli*. Applied and Environmental Microbiology, 72, 1164-1172.

Noriega, E., Velliou, E., Van Derlinden, E., Mertens, L., Van Impe, J.F.M., 2013. Effect of cell immobilization on heat-induced sublethal injury of *Escherichia coli*, *Salmonella* Typhimurium and *Listeria innocua*. Food Microbiology, 36, 355-364.

North, M.J., Collier, N.T., Ozik J., Tatara, E.R., Altaweel, M., Macal, C.M., Bragen, M., Sydelko, P., 2013. Complex Adaptive Systems Modeling with Repast Simphony. Complex Adaptive Systems Modeling, 1: 3.

Peaceman, D.W., Rachford, H.H., 1955. The numerical solution of parabolic and elliptic differential equations. Journal of the Society of Industrial and Applied Mathematics, 3, 28-41.

Schaechter, M., Williamson, J.P., Hood, J.R., Koch, A.L., 1962. Growth, cell and nuclear divisions in some bacteria. Journal of General Microbiology, 29, 421-434.

Thomas, L.H., 1949. Elliptic Problems in Linear Differential Equations over a Network. New York: Columbia University, Watson Scientific Computing Lab.

Trinh, C.T., Carlson, R., Wlaschin, A., Srienc, F., 2006. Design, construction and performance of the most efficient biomass producing *E. coli* bacterium. Metabolic Engineering, 8, 628-638.

Valgepea, K., Adamberg, K., Nahku, R., Lahtvee, P.-J., Arike, L., Vilu. R., 2010. Systems biology approach reveals that overflow metabolism of acetate in *Escherichia coli* is triggered by carbon catablite repression of acetyl-CoA synthetase. BMC Systems Biology, 4: 166.

Vemuri, G.N., Minning, T.A., Altman, E., Eiteman, M.A., 2005. Physiological response of central metabolism in Escherichia coli to deletion of pyruvate oxidase and introduction of heterologous pyruvate carboxylase. Biotechnology and Bioengineering, 90(1), 64-76.

Verhulst, A.J., Cappuyns, A.M., Van Derlinden, E., Bernaerts, K., Van Impe, J.F., 2011. Analysis of the lag phase to exponential growth transition by incorporating inoculum characteristics. Food Microbiology, 28, 656-666.

Volkmer, B., Heinemann, M., 2011. Condition-dependent cell volume and concentration of *Escherichia coli* to facilitate data conversion for systems biology modeling. PLoS ONE, 6: 7.

Wimpenny, J.W.T., Leistner, L., Thomas, L.V., Mitchell, A.J., Katsaras, K., Peetz, P., 1995. Submerged bacterial colonies within food and model systems: their growth, distribution and interactions. International Journal of Food Microbiology, 28, 299-315.

Wold, S., Skarstad, K., Steen, H.B., Stokke, T., Boye, E., 1994. The initiation mass for DNA replication in *Escherichia coli* K-12 is dependent on growth rate. The EMBO Journal, 13, 2097-2102.

Yanenko, N.N., 1971. The Method of Fractional Steps. Berlin: Springer.

Postprint version of paper published in Food Microbiology 2015, vol. 45(B), p. 179-188.
The content is identical to the published paper, but without the final typesetting by the publisher.

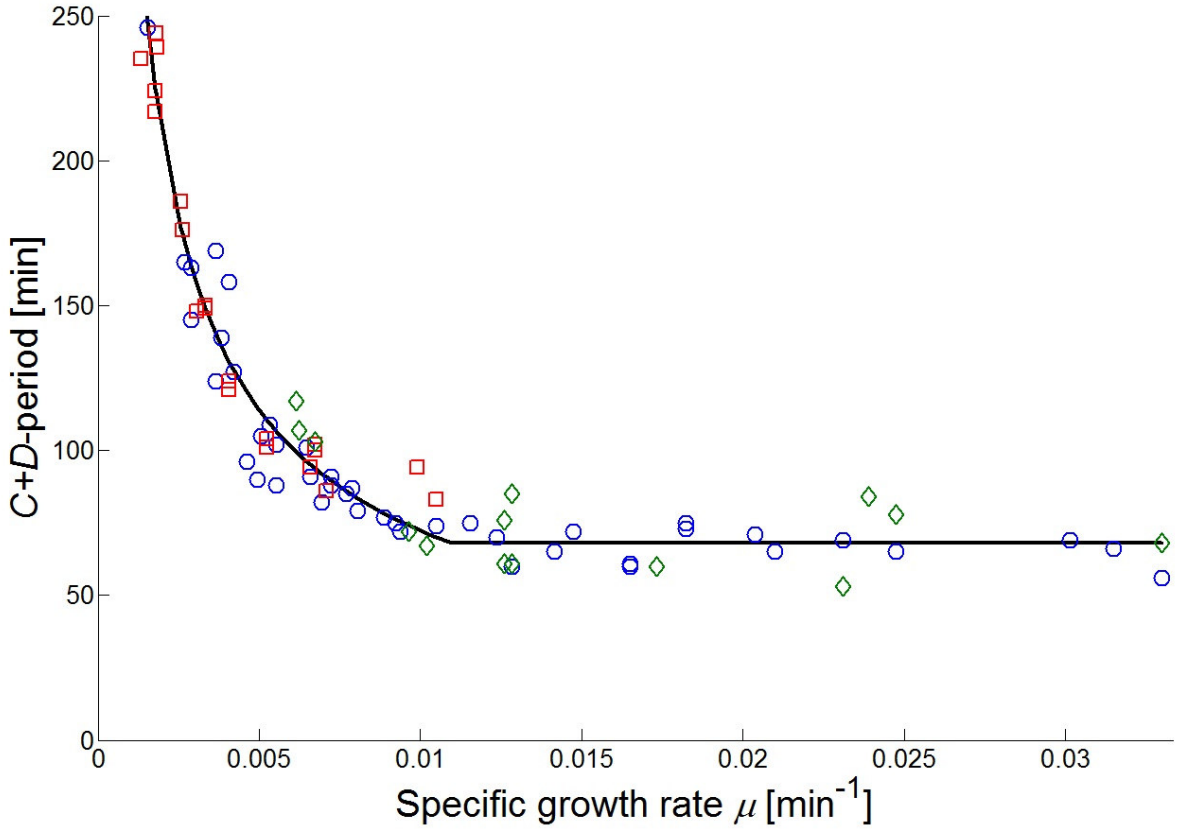

Figure 1: *C+D* period fitted as a function of specific cellular growth rate μ (MSSE = 13.93 min²). The symbols represent experimental batch data for *E. coli* K-12 listed in Table 3 of Michelsen et al. (2003) (o), chemostat data from Table 4 in Michelsen et al. (2003) (□), and *E. coli* K-12 data selected from Table 1 in Helmstetter (1996) (◊).

Journal homepage: http://www.sciencedirect.com/science/journal/07400020
Original file available at: http://www.sciencedirect.com/science/article/pii/S0740002014000963

Postprint version of paper published in Food Microbiology 2015, vol. 45(B), p. 179-188.
The content is identical to the published paper, but without the final typesetting by the publisher.

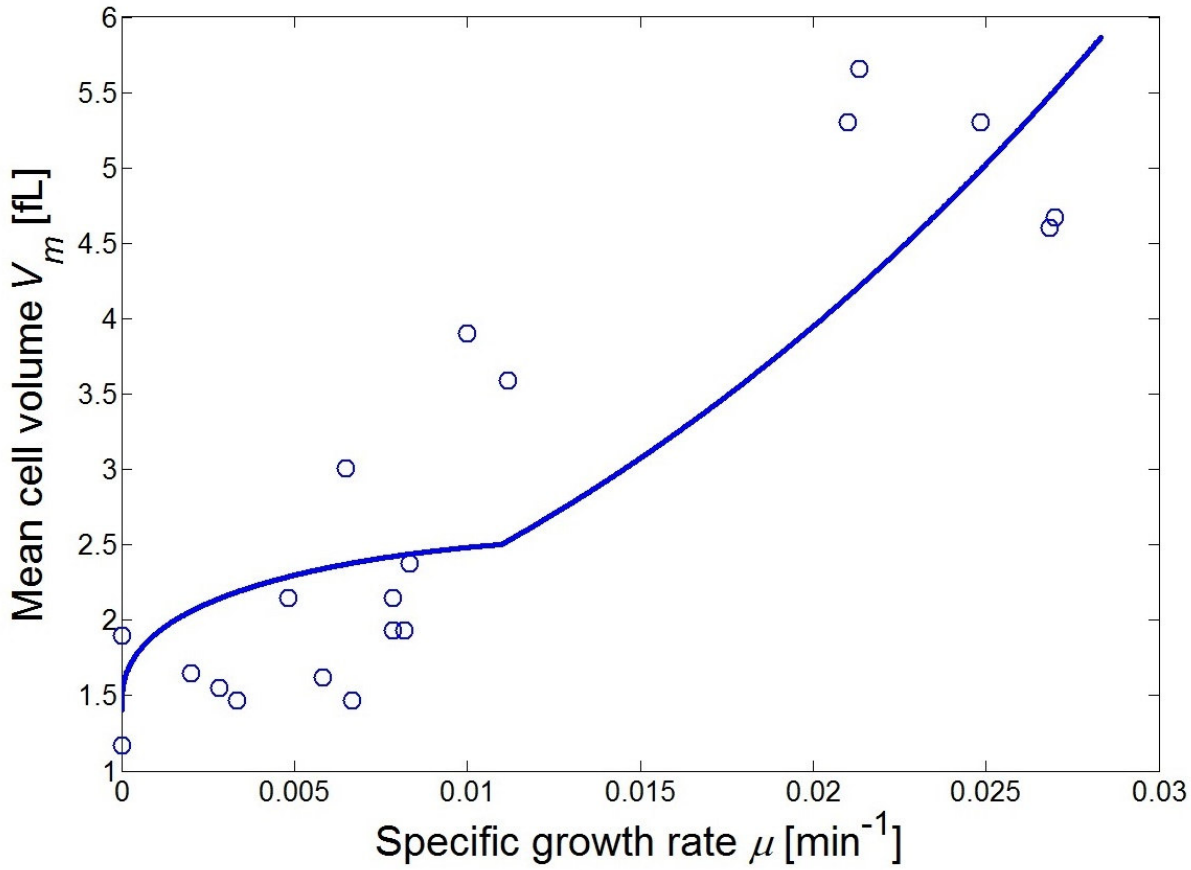

Figure 2: The critical initiation mass is calculated on the basis of the mean cell volume as a function of the specific cellular growth rate. Mean cell volume V_m as a function of specific cellular growth rate μ (MSSE = 5.9142 fL²). The experimental points (o) are calculated from the cell length (l) and width (w) data from Table 1 in Volkmer and Heinemann (2011), according to the mathematical expression $V_m = \pi \cdot w^2 \cdot (l - w/3)/4$ applicable to rod-shaped bacteria.

Journal homepage: http://www.sciencedirect.com/science/journal/07400020
Original file available at: http://www.sciencedirect.com/science/article/pii/S0740002014000963

Postprint version of paper published in Food Microbiology 2015, vol. 45(B), p. 179-188.
The content is identical to the published paper, but without the final typesetting by the publisher.

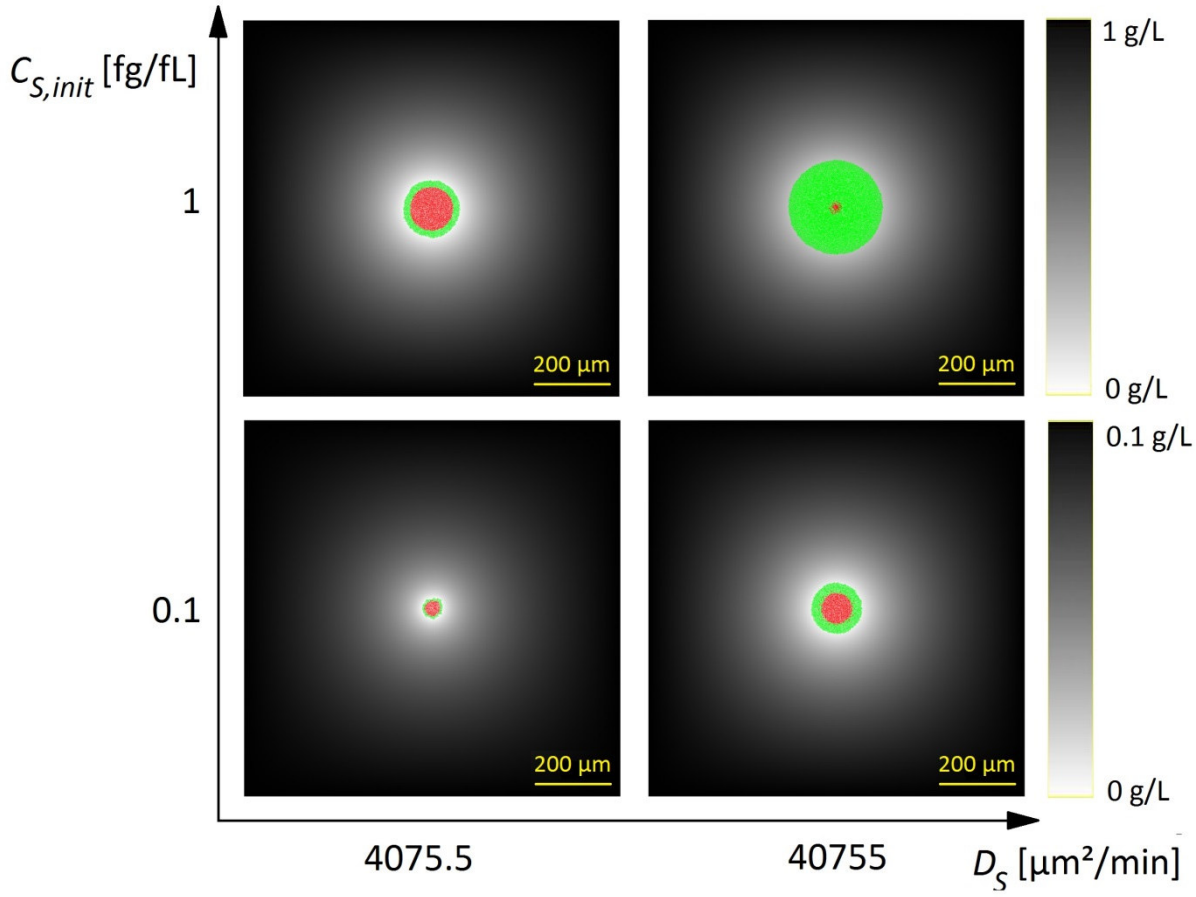

Figure 3: Influence of diffusivitiy D_S and initial glucose concentration $C_{S,init}$ on colony growth after 20 h. Local nutrient concentrations in the medium are represented by a grayscale; growing and starving cells by green and red dots, respectively. Lower diffusion coefficients (left plots) and lower initial nutrient concentrations (lower plots) lead to more severe nutrient depletion in the colony center and, consequently, smaller colonies with a larger fraction of starving cells.

Journal homepage: http://www.sciencedirect.com/science/journal/07400020
Original file available at: http://www.sciencedirect.com/science/article/pii/S0740002014000963

Postprint version of paper published in Food Microbiology 2015, vol. 45(B), p. 179-188.
The content is identical to the published paper, but without the final typesetting by the publisher.

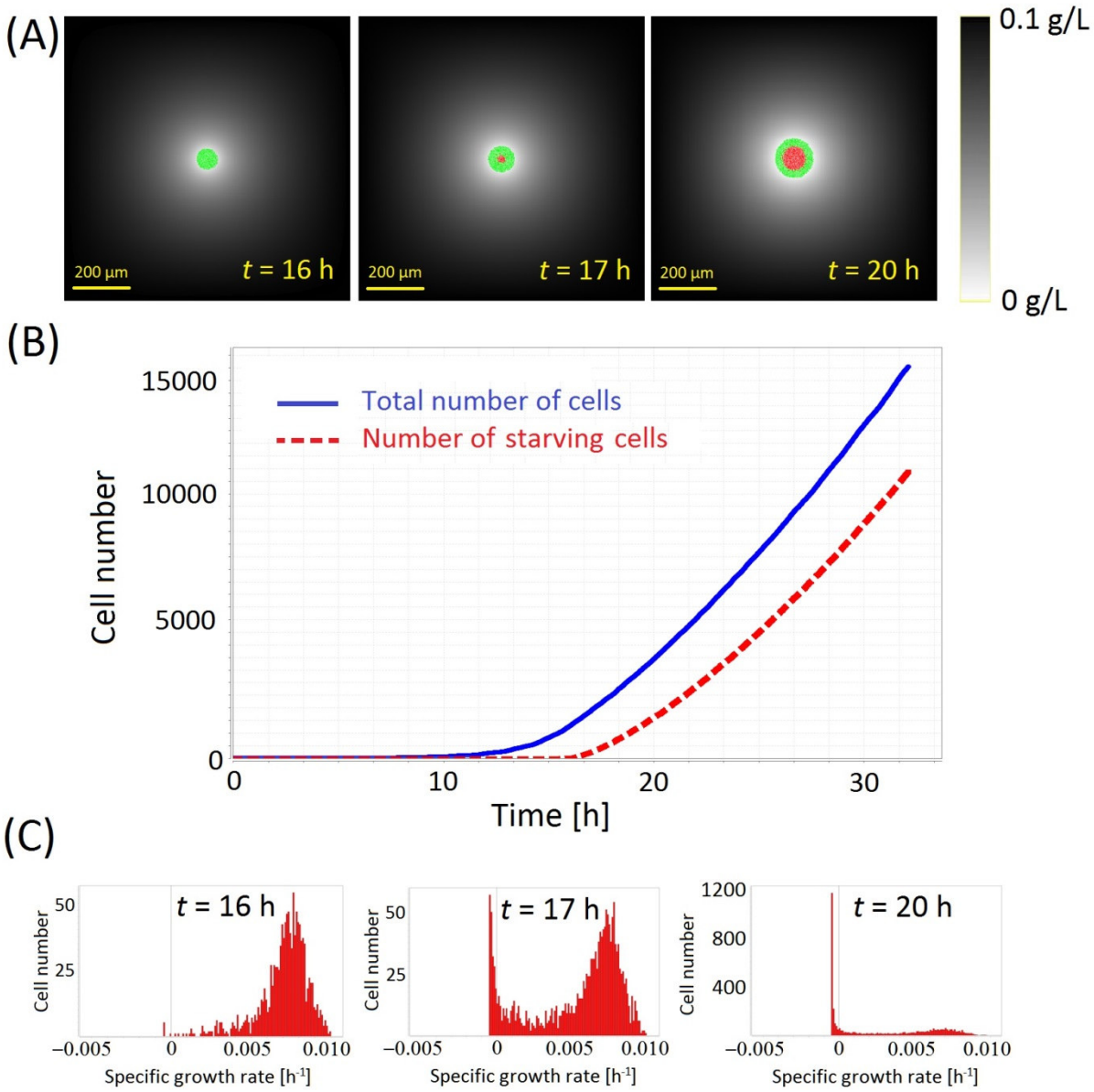

Figure 4: Emergence of the starvation zone (D_S = 40755 µm²/min, $C_{S,init}$ = 0.1 fg/fL, constant boundary conditions). (a) Cell starvation starts in the colony center and progresses towards the colony boundary. (b) The ratio of starving to growing cells increases monotonously over time. (c) The histogram of specific cellular growth rates depicts a bimodal distribution. Over time cells move from the right peak (positive specific cellular growth rate) to the left peak (negative specific cellular growth rate).

Journal homepage: http://www.sciencedirect.com/science/journal/07400020
Original file available at: http://www.sciencedirect.com/science/article/pii/S0740002014000963

Postprint version of paper published in Food Microbiology 2015, vol. 45(B), p. 179-188.
The content is identical to the published paper, but without the final typesetting by the publisher.

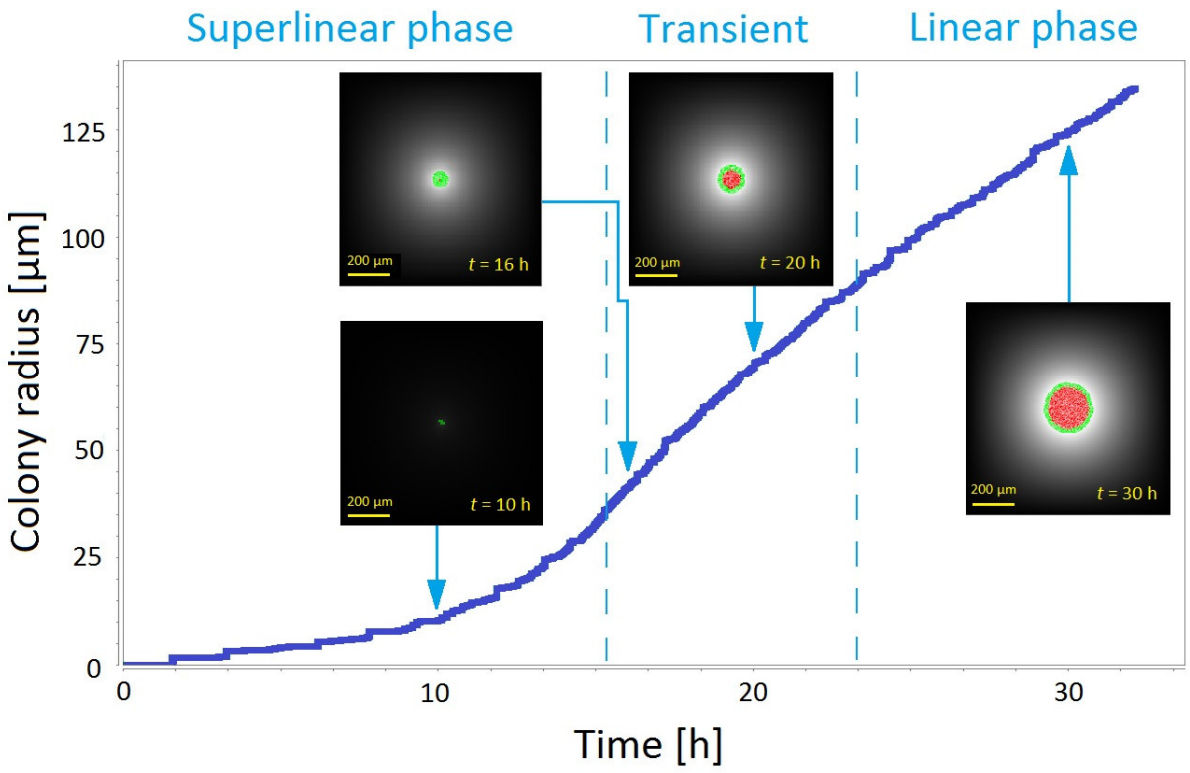

Figure 5: Evolution of the colony radius over time (D_S = 40755 µm²/min, $C_{S,init}$ = 0.1 fg/fL, constant boundary conditions). This evolution can be divided in three stages: a superlinear phase at the start of the experiment, a linear phase after nutrient depletion has become important, and a transition in between.

Journal homepage: http://www.sciencedirect.com/science/journal/07400020
Original file available at: http://www.sciencedirect.com/science/article/pii/S0740002014000963

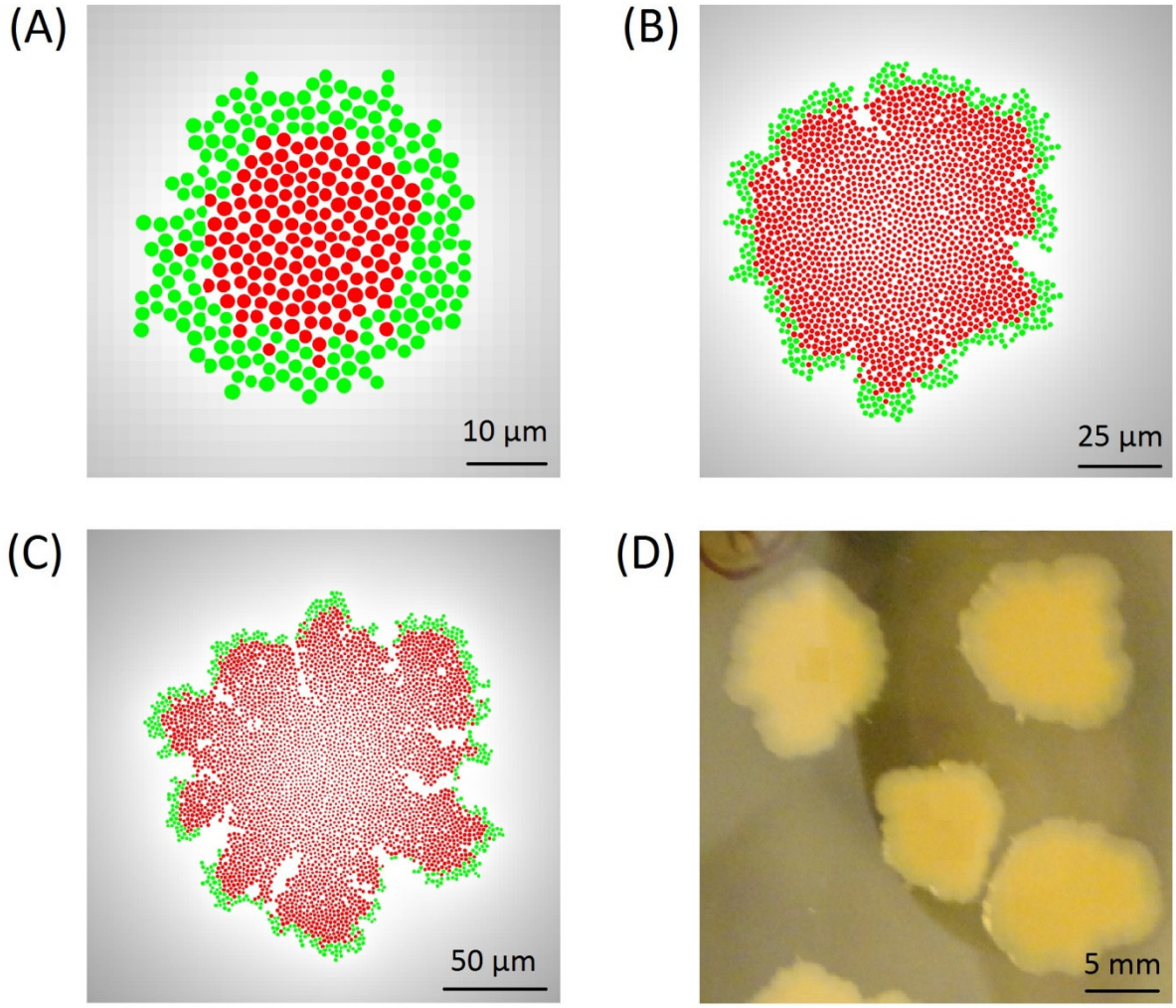

Figure 6: Evolution of the central zone of starving cells and the colony morphology (D_S = 4075.5 µm²/min, $C_{S,init}$ = 0.1 fg/fL, constant boundary conditions). (a) Disk-like morphology at t = 15 h, (b) Eden morphology at t = 40 h, and (c) dense branching morphology at t = 70 h. (d) For growth of *E. coli* K-12 MG1655 on Brain Heart Infusion supplemented with 10% (w/v) gelatin (higher D_S and $C_{S,init}$), the Eden morphology is experimentally observed at a larger spatial scale. (Unpublished photograph kindly provided by K. Boons, KU Leuven/BioTeC)

Journal homepage: http://www.sciencedirect.com/science/journal/07400020
Original file available at: http://www.sciencedirect.com/science/article/pii/S0740002014000963

Postprint version of paper published in Food Microbiology 2015, vol. 45(B), p. 179-188.
The content is identical to the published paper, but without the final typesetting by the publisher.

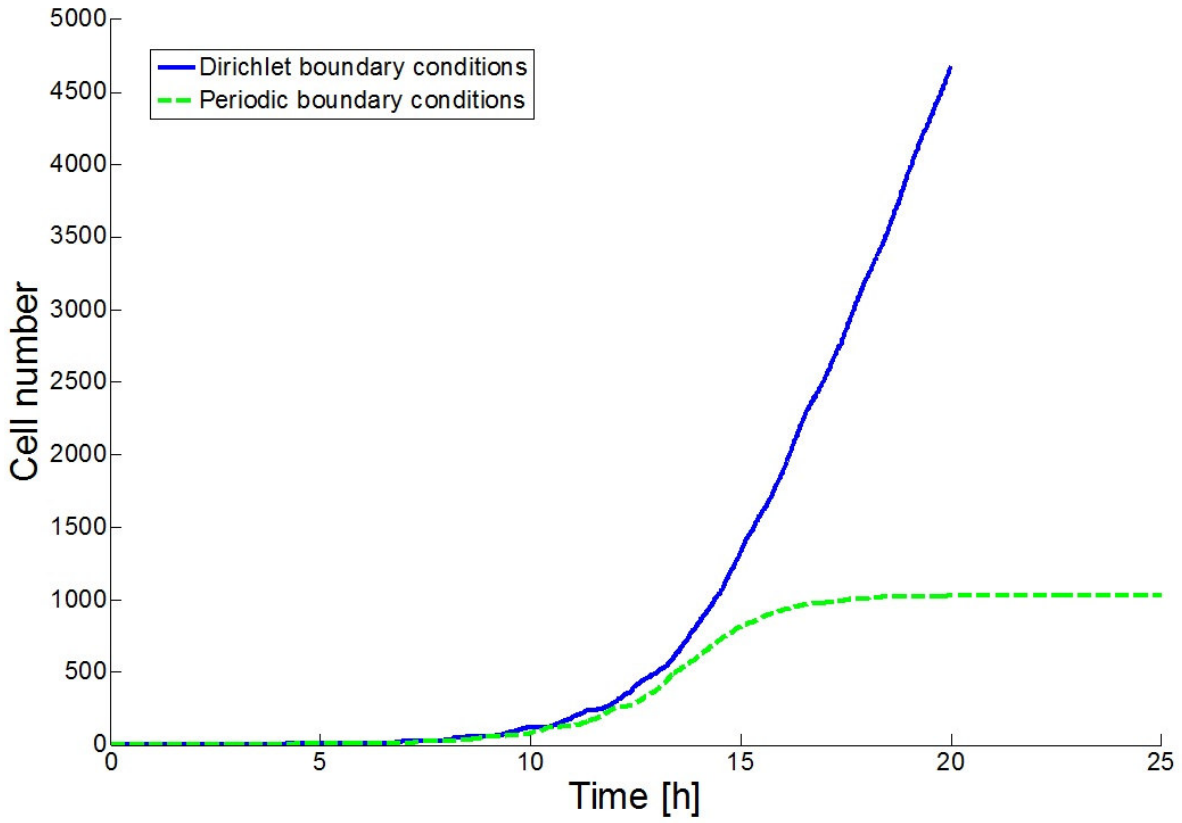

Figure 7: Stationary phase behavior of microbial colonies is incorporated in the model by means of periodic boundary conditions (D_S = 40755 µm²/min, $C_{S,init}$ = 1.0 g/L).

Journal homepage: http://www.sciencedirect.com/science/journal/07400020
Original file available at: http://www.sciencedirect.com/science/article/pii/S0740002014000963

Postprint version of paper published in Food Microbiology 2015, vol. 45(B), p. 179-188.
The content is identical to the published paper, but without the final typesetting by the publisher.

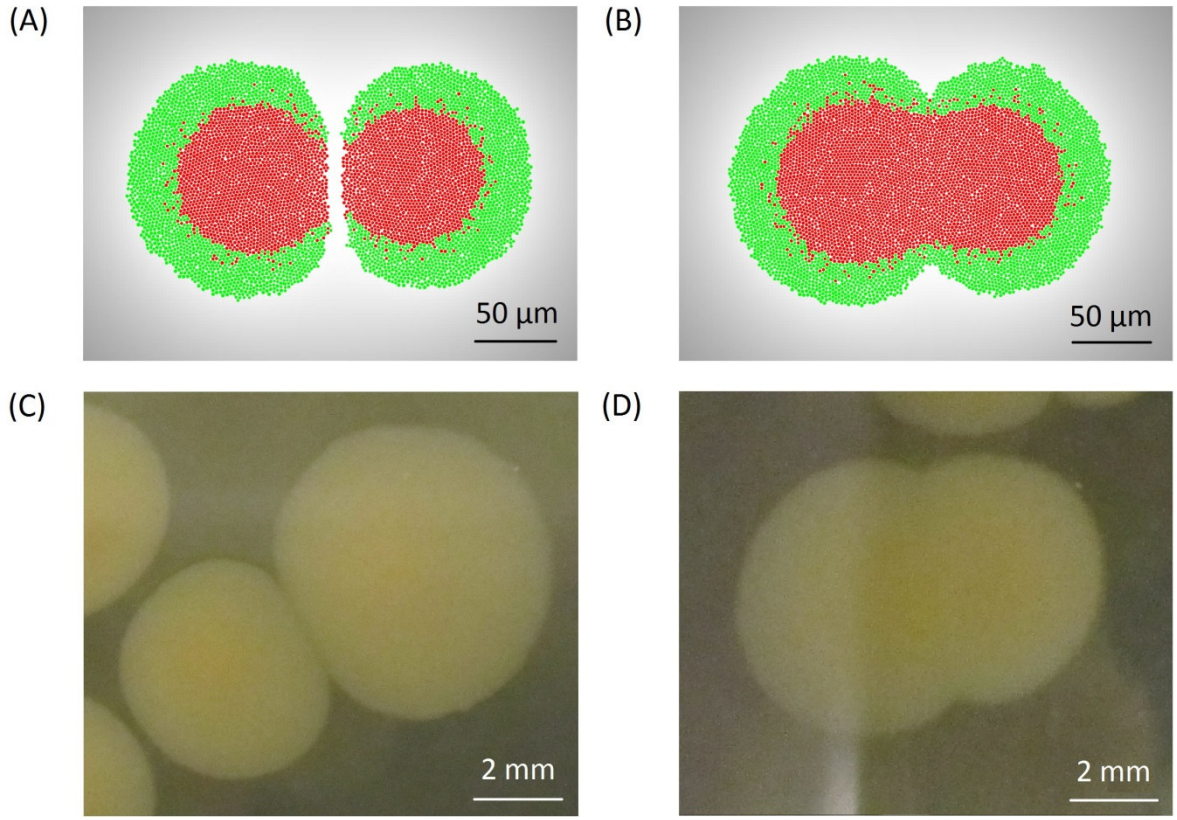

Figure 8: Interaction between two neighboring colonies (D_S = 40755 µm²/min, $C_{S,init}$ = 0.1 fg/fL, constant boundary conditions). (a) Colony repulsion at an inoculum distance *d* of 80 µm. (b) Colony merging at *d* = 60 µm. (c,d) For growth of *E. coli* K-12 MG1655 on BHI supplemented with 1.2% (w/v) agar (higher $C_{S,init}$), colony repulsion and merging are experimentally observed at a larger spatial scale. (Unpublished photographs kindly provided by E. Noriega Fernández)

Journal homepage: http://www.sciencedirect.com/science/journal/07400020
Original file available at: http://www.sciencedirect.com/science/article/pii/S0740002014000963

Postprint version of paper published in Food Microbiology 2015, vol. 45(B), p. 179-188.
The content is identical to the published paper, but without the final typesetting by the publisher.

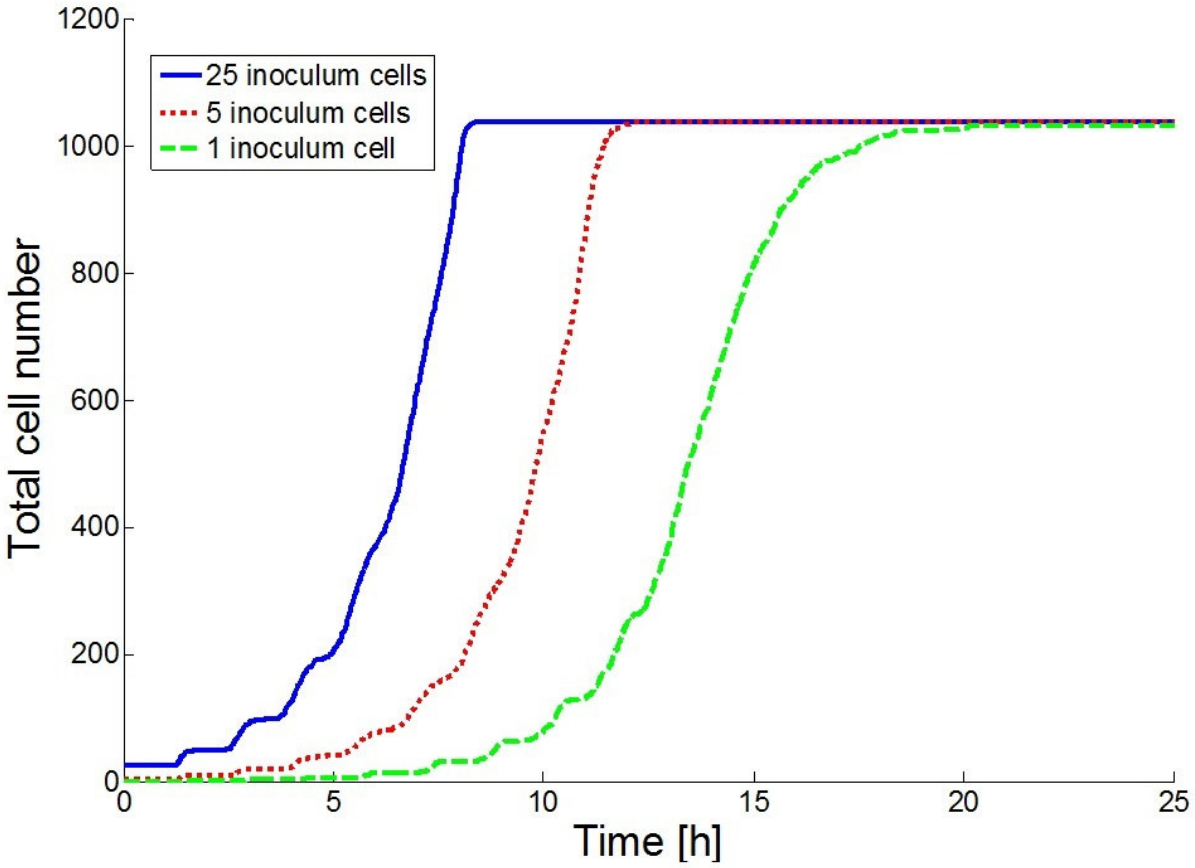

Figure 9: Mutual influence of multiple colonies (D_S = 4075.5 µm²/min, $C_{S,init}$ = 1.0 fg/fL, periodic boundary conditions). Higher inoculum densities lead to smaller colonies, as nutrient competition becomes more severe. The maximum number of cells is hardly influenced by the inoculum density.

Journal homepage: http://www.sciencedirect.com/science/journal/07400020
Original file available at: http://www.sciencedirect.com/science/article/pii/S0740002014000963

Postprint version of paper published in Food Microbiology 2015, vol. 45(B), p. 179-188.
The content is identical to the published paper, but without the final typesetting by the publisher.

Table 1: Cellular parameter values for *Escherichia coli* K-12 MG1655 applied in the IbM simulations.

Symbol	Explanation	Value[a]	Reference
α	Ratio of mean cell mass to cell mass at birth	1.377	Koch (1993)
$\mu_{max,m}$	Mean maximum specific cellular growth rate	0.0082 min^{-1}	Trinh et al. (2006)
		0.0090 min^{-1}	Valgepea et al. (2010)
		0.0093 min^{-1}	Baumler et al. (2011)
		0.0088 min^{-1}	current work
ρ	Density of cellular biomass	1160 fg/fL	Godin et al. (2007)
ρ_{DW}	Density of dry cellular biomass (ρ·(1-*CWC*))	301.6 fgDW/fL	
A	Critical initiation ratio at μ = 0 h^{-1}	610.7 fgDW	Volkmer and Heinemann (2011)
B	Linear decrease factor of *X** with respect to μ	8315.1 fgDW·min	Volkmer and Heinemann (2011)
CV	Coefficient of variance of specific growth rate	0.10	Schaechter et al. (1962)
		0.10	Koch (1993)
		0.10	current work
CWC	Cellular water content	74%	Kamihira et al. (1987)
K_S	Monod half-saturation constant	0.539·10^{-3} fg/fL	Ihssen et al. (2007)
m	Maintenance coefficient	8.0·10^{-4} fg/(fgDW·min)	Vemuri et al. (2005)
		11.1·10^{-4} fg/(fgDW·min)	Nanchen et al. (2006)
		10.5·10^{-4} fg/(fgDW·min)	Esquerré et al. (2013)
		9.9·10^{-4} fg/(fgDW·min)	current work
s	Intercellular distance in cell shoving mechanism	1.3	Kreft et al. (1998)
$Y_{X/S}$	Biomass yield coefficient	0.45 fgDW/fg	Trinh et al. (2006),
		0.44 fgDW/fg	Ihssen et al. (2007),
		0.45 fgDW/fg	Baumler et al. (2011)
		0.45 fgDW/fg	current work

Journal homepage: http://www.sciencedirect.com/science/journal/07400020
Original file available at: http://www.sciencedirect.com/science/article/pii/S0740002014000963

[a] All cellular parameter values are valid for *Escherichia coli* K-12 MG1655 cells in an aerobic environment at 37°C and neutral pH. In case of multiple references, the parameter value is taken as the arithmetic mean of the found values (indicated in bold).